Simulation of UWB Distortion Combined with Indoor Spatio-Temporal Channels

K. Makaratat, S. Stavrou, T.W.C. Brown

CCSR University of Surrey, Guildford Surrey, GU2 7XH, United Kingdom
Email: K. Makaratat@surrey.ac.uk

Abstract

The modified aspects for simulating UWB multipath channels are presented in this paper. Pulse distortion mechanisms based on the geometric optics and the geometric theory of diffraction are specifically generated combing with the spatio-temporal characteristics of multipath clusters based on 3x3 planar array systems. In each particular scenario, model parameters such as angle-of-arrival, angle-of-departure and time-of-arrival are statistically synthesized, corresponding to cluster groups along the propagation paths. Furthermore, characteristics of frequency dependence of propagation channels simulated over 10 frequency subbands (2-11 GHz) with 1 GHz bandwidth are also analysed.

1 Introduction

In order to investigate Ultra Wideband (UWB) channel modeling, its propagation paths are characterized as the stationary condition where the channel characteristics remain constant within limited space, time, and frequency intervals. All multipath information should be taken into account to support realistic UWB propagation channels. Various works in channel investigations discuss about UWB multipath clusters and their dependency on measurement bandwidth and the considered environment. In general, the UWB multipath cluster model is described by the classical Saleh-Valenzuela (SV) model [1] and by some modifications as proposed by Chong *et al.* [2] and Spencer *et al.* [3] where, in the latter, the combined spatio-temporal statistical model for indoor multipath propagation was presented herein. Furthermore, some research proposed a generic statistical channel model for a wideband environment [4] including the frequency dependent characteristics such as angular/delay spreads. However, these UWB channel model simulations imply only channel impulse responses (CIRs) without any details of multipath clusters and distortion effects.

This paper investigates both the geometrically-based pulse distortion model and the UWB spatio-temporal channel statistics by combining physics-based pulse distortions and UWB multipath clusters captured by planar arrays. This proposed simulation also gain the advantage of investigating the UWB CIRs with a short simulation time due to generating only specific dominant multipath signals.

2 Physics-based pulse distortion characteristics

According to UWB channel properties for multipath, more than one multipath ray can be observed within a short time bin. These overlapped ray arrivals essentially originate from the same propagation routes and can inevitably cause pulse shape distortions. As a result, this section describes an UWB time-domain distortion model, based on geometric optic (GO) technique to describe direct and reflected rays, and based on geometric/uniform theory of diffraction (GTD/UTD) technique to describe the diffracted rays. Typically, the total response, $h(\tau)$, from a complex multipath channel can be modeled by the summation of all impulse responses of local scattering with the closed form expression of specific geometric configurations as presented in (1) [5].

$$h(\tau) = h(\tau,\theta,\phi) = \sum_{n=1}^{N_{GO}} a_n(\theta,\phi)\cdot\delta(\tau-\tau_n) + \sum_{n=1}^{N_d} h_n(\tau,\theta,\phi)\otimes\delta(\tau-\tau_n) \quad (1)$$

where N_{GO} and N_d are the geometric-optic-ray and diffracted-ray-numbers respectively. In general, three significant propagation mechanisms which cause physics-based distortion in UWB propagation channels are considered: geometric optic (GO) rays (LOS connection), diffracted rays due to a half plane, and finally, diffracted rays by a dielectric slab [6]. Illustration of UWB pulse distortion mechanisms is also illustrated in Fig. 1.

2.1 Geometric Optic Rays and Multiple Reflections

In practical, the distortion due to GO rays can be simply presented by the general M-different-reflection model, as can be defined by [5-6].

$$h(\tau) = \frac{1}{r_{direct}}\delta(\tau) + \frac{1}{r_{reflect}} R_M(\tau)\otimes\delta(\tau-\tau_M) \quad (2)$$

where $R_M(\tau) = K^M\delta(\tau) + MK^{M-1}R_{01} + \sum_{m=2}^{M}\frac{M!}{(M-m)!m!}K^{M-m}$. $F_{0m}(k,\tau)$. M is the number of different reflections. R_{01} and $F_{0m}(k,\tau)$ can be derived as in the Appendix B in [6]. $K=(1-k)/(1+k)$ and $k=\sqrt{\varepsilon_r-\cos^2\theta_r}/\varepsilon_r\sin\theta_r$ or $k=\sin\theta_r/\sqrt{\varepsilon_r-\cos^2\theta_r}$ for vertical or horizontal polarization respectively with $\theta_r = \arctan((h_{tx}+h_{rx})/d)$. $\tau_1 = (r_{reflect} - r_{direct})/c$, $a = 120\pi\sigma c/(2\varepsilon_r)$ where ε_r is a relative dielectric constant and σ is the conductivity of the reflecting surface.

2.2 Diffraction by a perfectly conducting half-plane

This diffraction phenomena is commonly produced by edges of tables, counters, other furniture etc. as shown in Fig. 1. For any incident angle θ_i' at a half plane, the impulse response can be expressed by [6]

$$h_{half-plane-diffract}(\tau) = \sqrt{2r/c}/2\pi \left[\frac{\cos((\theta_r' - \theta_i')/2)}{\tau + \frac{r}{c}\cos(\theta_r' - \theta_i')} - \frac{\cos((\theta_r' - \theta_i')/2)}{\tau + \frac{r}{c}\cos(\theta_r' - \theta_i')} \right] \times \frac{1}{\sqrt{\tau - r/c}} U(\tau - r/c) \quad (3)$$

2.3 Propagation through d-thickness-slab obstructions

This propagation mechanism can be generally observed in UWB propagating through walls, doors, partitions, etc. Transmitted pulses can be transmitted, reflected or even diffracted by a thin slab in different regions. Moreover, multiple reflections and transmissions are generated when propagating through thick walls or obstacles. The closed form time-domain expressions of the total transmission coefficient, $T_{slab}(\tau)$, and the total reflection coefficient, $R_{slab}(\tau)$, for propagation through any d-thickness slabs can be derived as,

$$T_{slab}(\tau) = \delta(\tau - \tau_{2,1}) + R_2(\tau)[\delta(\tau - \tau_{1,1}) - \delta(\tau - \tau_{2,1})] + \sum_{n=2}^{\infty} R_{1,2n}(\tau) \otimes \delta(\tau - \tau_{1,n}) - \sum_{n=1}^{\infty} R_{1,2n}(\tau) \otimes \delta(\tau - \tau_{2,n}) \quad (4)$$

where $\tau_{1,n}=2(-\sqrt{\varepsilon_r}+\sin\theta_t \sin\theta_i)nl/c$ and $\tau_{2,n}=[-(2n-1)\sqrt{\varepsilon_r} + (2n-2)\sin\theta_t\sin\theta_i+\cos(\theta_i-\theta_t)]nl/c$ with $l=d/\cos\theta_t$ and d is thickness of a slab [6].

$$R_{slab}(\tau) = -R_1(\tau)[\delta(\tau) + \delta(\tau - \tau_1)] - \sum_{n=2}^{\infty} R_{1,2n-1}(\tau) \otimes \delta(\tau - \tau_n) + \sum_{n=1}^{\infty} R_{1,2n+1}(\tau) \otimes \delta(\tau - \tau_n) \quad (5)$$

where $R_{1,M}(\tau)=K_1^M\delta(\tau)+MK_1^{M-1}R_{01}(\tau)+\sum_{m=2}^{M} M!/((M-m)!m!)\cdot K_1^{M-m}F_{0m}(k_1, \tau)$; $M\geq 1$, and $\tau_n=2(1+\sin\theta_t \sin\theta_i)nl/c$. Additionally, if UWB pulses propagate through a thin thickness slab, the total diffraction coefficient, $D_{slab}(\tau)$, will be considered as shown in (6).

$$D_{slab}(\tau) = 1 - T_{slab}(\tau) \otimes D_{half-plane}(\tau, \theta_d - \theta_i) + R_{slab}(\tau) \otimes D_{half-plane}(\tau, \theta_d + \theta_i) \quad (6)$$

where $D_{half\text{-}plane}(\tau,\theta_d \mp \theta_i) = -L\cos((\theta_d \mp \theta_i)/2)/\{2\pi\sqrt{2c\tau}(\tau+L/2c \cos^2((\theta_d \mp \theta_i)/2))\}$. These pulse distortion characteristics will be combined into the IEEE UWB CIR which will be described in the next section.

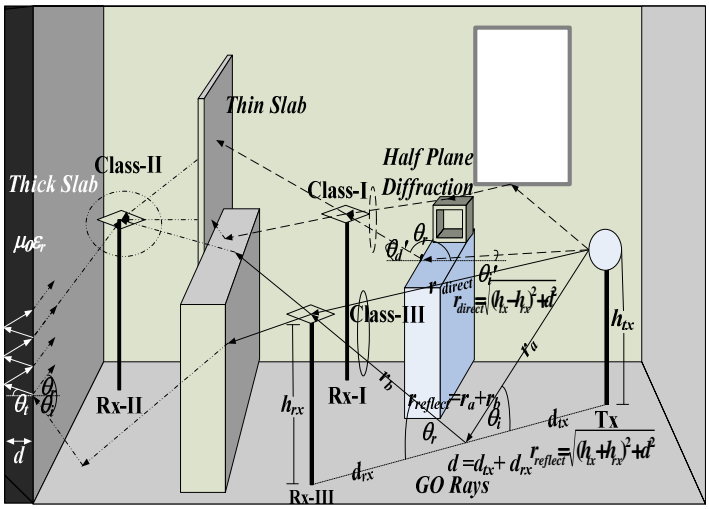

Fig. 1. Illustration of distortion mechanisms and classification of UWB multipath clusters

3 Classification of UWB multipath clusters and channel impulse response modelling

3.1 Classification of UWB multipath clusters

According to multipath cluster investigations derived from indoor UWB measurements [1-3], [7-8], each multipath cluster could be identified by a group of multipath components (MPCs) which are scattered from obstructions with similar AOAs, AODs, and TOAs. The received multipath clusters from dominant propagation paths from a transmitter to a receiver are expected to come from three types of propagation paths. The first group corresponds to scattering nearby the transmitter. Similarly, another group can be observed at the receiver site due to the scattering objects in the neighboring area of the receiver. Finally, line-of- sight (LOS) components between the transmitter and the receiver are considered. Consequently, these different propagation clusters can be classified into three classes as Class-I, Class-II and Class-III type of clusters respectively [4] as illustrated in Fig. 1 where the omnidirectional antenna is considered as the transmitter, and 3x3 planar array antenna is the receiver.

When defining significant clusters specifically related to propagation scenarios, in the LOS scenario of Case-A describing a small furnished office room, the channel would be dominated by Class-III clusters. Next, the NLOS scenario Case-B is considered where a transmitter and a receiver are in the same office room with a-light-wall or a-cloth-partition separation between both ends; the channel would be still dominated by Class- III cluster. However, when propagation paths in a larger furnished office room -NLOS scenario Case-C- are considered, all three classes of clusters are presented. Finally, if a transmitter and a receiver are located in a different furnished room or separated by a thick wall, the channel would be dominated by Class-I and Class-II clusters corresponding to the extreme NLOS condition (Case-D). Types and numbers of dominated clusters corresponding to each scenario are also described in Table I.

3.2 Channel Impulse Response Modeling

Extending the work of the previous simulation model [4], inter-cluster and intra-cluster characteristics are also examined. Several statistics such as AOAs, AODs, TOAs, Power Angular Spectrum (PAS), Power Delay Spectrum (PDS), etc., have to be known first in order to parameterize the models. These parameters can be obtained from various channel measurements [1-3], [7-8]. Consequently, LOS Case-A and NLOS Case-B, Class-III cluster-CIRs are taken into account and CIRs are described by (7) and (8) respectively.

$$h_{case-A}(s,t;\tau,\phi) = h_{LOS}(s,t;\tau,\phi) + h^{III}(s,t;\tau,\phi) \quad (7)$$

$$h_{case-B}(s,t;\tau,\phi) = h_{LOS}(s,t;\tau,\phi) + h^{III}(s,t;\tau,\phi) \quad (8)$$

$$h(s,t;\tau,\phi) = \sum_{l=1}^{L(s,t)} \sum_{k=1}^{K(l)} \sqrt{P_{k,l}(s,t)} \cdot \delta\left(\tau - T_l(s,t) - \tau_{k,l}(s,t), \phi - \Phi_l(s,t) - \phi_{k,l}(s,t)\right) \quad (9)$$

s is the index of the UWB subband channel divided from the entire frequency spectrum. $L(s,t)$ is the number of clusters for the sth subband channel at time instant t and $K(l)$ is a total number of multipath components (MPCs) in the lth cluster. $T_l(s,t)$ and $\Phi_l(s,t)$ are the TOA and the mean of all angles of arriving contributions of the lth cluster respectively. $\tau_{k,l}(s,t)$ and $\phi_{k,l}(s,t)$ are the delay and the AOA of the kth MPC in the lth cluster respectively. $P_{k,l}$ is the average power of the kth MPC in the lth cluster including of PDS and PAS of intercluster statistics, $p_{Inter}(T_l, \Phi_l | T_{l-1}, \Phi_0) = p(T_l|T_{l-1}) \cdot p(\Phi_l|\Phi_0)$, and intracluster statistics, $p_{Intra}(\tau_{k,l}, \phi_{k,l} | \tau_{k-1,l}) = p(\tau_{k,l}|\tau_{k-1,l}) \cdot p(\phi_{k,l})$.

The CIR term for LOS components which is considered in (1) and (2) is defined by $h_{LOS}(s,t;\tau,\phi) = \sqrt{P_{LOS}(s,t)} \cdot \delta(\tau - d(t)/v_c, \phi - \phi_{LOS}(t))$ where P_{LOS} is the power of LOS component, d is the distance between both ends, $v_c = 3\text{x}10^8$ m/s and ϕ_{LOS} is the AOA of the direct path. Next, for the impulse response of the Case-C and Case-D NLOS scenarios can be determined by

$$h_{case-C}(s,t;\tau,\phi) = h^{III}(s,t;\tau,\phi) + h^{II}(s,t;\tau,\phi) + g^{I}(s,t;\phi_{Tx}) \quad (10)$$

$$h_{case-D}(s,t;\tau,\phi) = h^{II}(s,t;\tau,\phi) + g^{I}(s,t;\phi_{Tx}) \quad (11)$$

where $g^I(s,t;\phi_{Tx})$ is the single-directional-channel response of Class-I clusters at the transmitter site.

$$g^{I}(s,t;\phi_{Tx}) = \sum_{m=1}^{M(s,t)} \sum_{n=1}^{N(m)} \sqrt{P_{n,m}(s,t)} \times \left(\phi_{Tx} - \phi_{Tx,n,m}(s,t)\right) \quad (12)$$

$M(s,t)$ is the number of Class-I clusters for the sth subband channel at time instant t and $N(m)$ is the number of AODs in the mth Class-I cluster. $\phi_{Tx,n,m}(s,t)$ is the AOD of the nth MPC in the mth cluster, and finally, $P_{n,m}$ is the average power of the nth MPC in the mth cluster which is determined by PAS.

4. Modified spatio-temporal simulation and simulated results

4.1 Modified Spatio-Temporal Simulation

This section proposed an UWB pulse simulation method based on planar array systems, a different approach than the one proposed in [4] by incorporating the physics-based pulse distortion model. Using priori modeled parameters [1-3], [7-8], which are presented in Table I, the structure of this simulation can be described as follows with a uniform distribution denoted in some parameters. Firstly, the entire frequency (2-11 GHz) will be divided into 10 subbands with each subband occupying 1 GHz bandwidth. CIRs and distorted pulses are generated representing the arrival rays with the UWB transmitted pulse consists of the second derivative of a Gaussian function $W(\tau) = \tau \exp(-2\pi[\tau/\tau_n]^2)$. All following processes are applied to each subband. Next, the propagation scenario of interest for instances Case-A, Case-B, Case-C or Case-D is specified, and the cluster numbers of each associated cluster class corresponding to the environment conditions are generated. Then frequency-dependent AS ($\sigma_{\phi,s}$) and DS ($\sigma_{\tau,s}$) for each s-subband are defined, where $\sigma_{\phi,s} = \beta_\phi \exp(\gamma_\phi f_{centre,s})$ and $\sigma_{\tau,s} = \beta_\tau \exp(\gamma_\tau f_{centre,s})$. $f_{centre,s}$ is the centre frequency of each subband. Finally, the discrete AODs, AOAs and TOAs are generated using the method of equal areas (MEA) [4].

Moreover, when Cluster-I and Cluster-II are considered, it is assumed that the AODs represent the incident angles of the transmitted signal when propagating through the obstructions. Additionally, azimuth AOAs represent arriving angles arising from diffraction or reflection contributions from horizontal directions, and elevation AOAs represent diffracting or reflecting angles coming from vertical directions.

Consequently, using this methodology, UWB multipath CIRs and their distorted pulses can be generalized based on specific environments. Modeling parameters and types of distortion mechanisms in Table I are selected corresponding to propagation path cases and related classes of clusters. The height of the transmitter and the receiver is 1.325 m. The time resolution of generated signals in this simulation is 83.32 ps with 6144 data points. Accordingly, the maximum time delay allocating MPCs is approximately 500 ns. However, very low level of some generated impulse signals are not considered although they appear earlier than 500 ns.

4.2 Simulation Results

Since a whole 9-frequency-subband received signals are simulated with 3x3 planar arrays, this can lead to complex and congested results (81 values for one MPC). Hence only simulating results from one frequency subband observed by the reference (3,3) antenna are shown here. Fig. 2 depicts the examples of generalized 5 UWB MPCs arriving at the receiver at 30, 34, 55, 123 and 175 ns respectively. The first arrival path represents a LOS received signal with AOA=81°. The second component represents the 3-multiple reflection

Table I Simulating model parameters for distorted UWB CIR

Scenario Cases	Dominant Cluster Classes/ Distortion Mechanisms	Simulating Channel Parameters									
		Cluster No, L	MPC No, K	β_ϕ	β_θ	β_τ	$\gamma_\phi, \gamma_\theta$	γ_τ	τ_0	γ	Γ
LOS-A (3-18 m)	Class-III / GO, M-reflection, Half-plane diffraction	[1,5]	[1,3]	[0,5]	[0,5]	[0,2]	0	0	[10,60]	4.3	7.1
NLOS-B (3-18 m)	Class-III / GO, M-reflection, Half-plane diffraction, Thin slab diffraction	[3,7]	[1,5]	[5,10]	[0,5]	[0,20]	[-0.1,0]	0	[10,60]	6.7	5.5
NLOS-C (9-30 m)	Class-III / GO, M-reflection, Half-plane diffraction	[3,7]	[1,5]	[10,30]	[0,5]	[10,40]	[-0.1,0]	0	[30,100]	7.9	14
	Class-I+II / Thin slab diffraction, Thick slab reflection	[5,10]	[5,10]								
NLOS-D (>18 m.)	Class-I+II / Thick slab reflection	[5,10]	[5,10]	[30,50]	[0,5]	[20,80]	[-0.1,0]	0	[60,200]	12	24

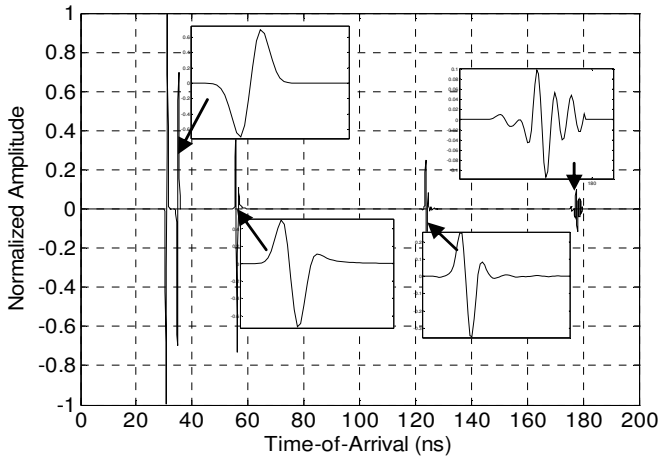

Fig. 2. Examples of pulse distortions due to various mechanisms

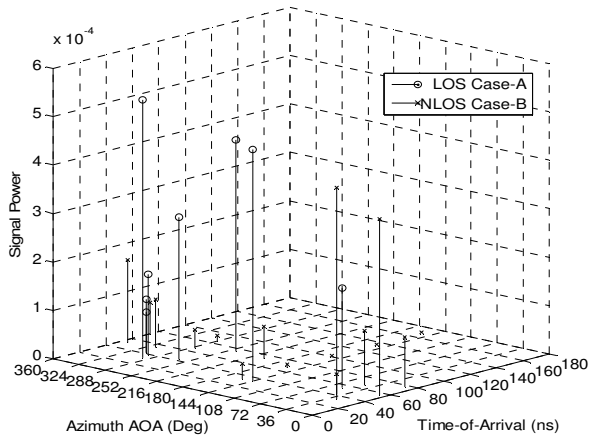

(a) 3D Channel impulse responses

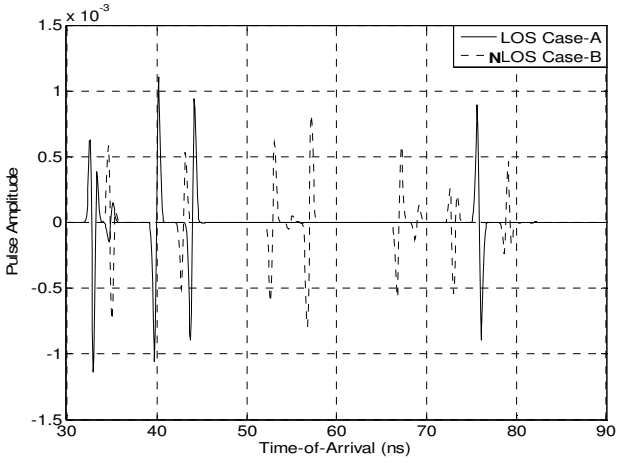

(b) Simulated pulse signals

Fig. 3. Comparison of received signal simulation between LOS Case-A and NLOS Case-B

signal between two wallboards located both sides along the propagation path to the receivers. It is assumed that reflected angles between both wallboards are identical with 87°. The third MPC is specified as the diffraction from an aluminium side of a bookcase with r = 3.2 m. and $\theta_d^{'}$= 87°. When considering propagation through a thin slab obstruction, a wooden door (d= 4.44 cm.) with θ_d= θ_i= 76°, the sample of the distorted pulse is illustrated as the fourth MPC. Finally, the distortion due to propagation through a thick slab such as a concrete wall (d=19.45cm.) can be shown in the last MPC.

Fig. 3 presents the comparison of simulated results of LOS Case-A and NLOS Case-B operating at 6 GHz. In Fig. 3(a), CIRs are plotted in three dimensional views of azimuth AOAs and TOAs. In Fig. 3(b), received pulse signals for LOS Case-A, are simulated as a direct path signal with a reflection from a floor and also multiple reflections from surrounding obstructions. The aluminum plate is considered as the half plate from which signals diffract to the receiver. Furthermore, simulated UWB pulse signal propagating in an office room (NLOS Case-B) where some areas are separated by a thin wallboard (d=1.17 cm) and a cloth partition (d=5.93 cm) is also presented in this figure. MPCs in Case-A are less than Case-B but with stronger strength of received signals. Signal arrivals at 65 ns, 73 ns and 78 ns present propagations through a cloth partition and a wallboard respectively. In addition, UWB propagation in a larger office room where a thick wall is located along propagation paths, NLOS Case-C, is simulated and its results are shown in Fig. 4. This scenario consists of all three classes of clusters. According to the characteristics of clusters, Class-III clusters are dominated by the direct signals, single reflection and multi-reflection between LOS connections. Therefore, its signal strength, indicated by a solid line, is higher than pulse signals

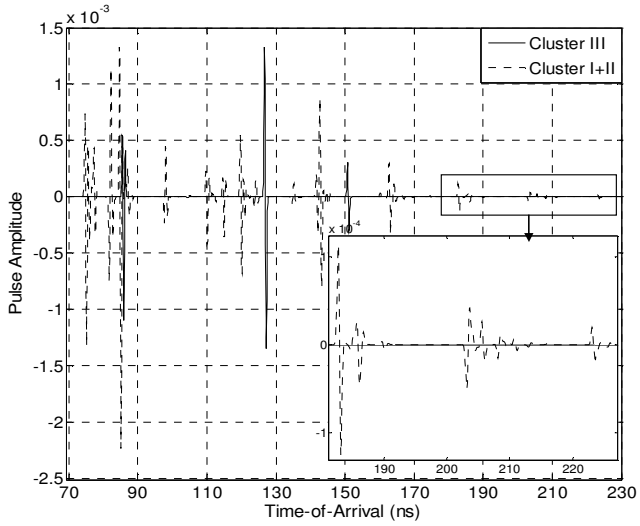

Fig. 4. Simulated pulse signals for NLOS Case-C

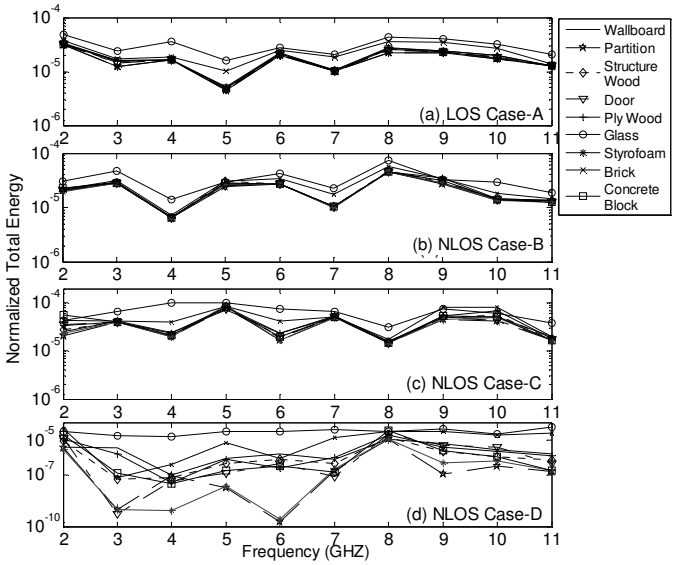

Fig. 5. Comparison of total energy variations for all frequency subbands

dominated by Class-I and Class-II clusters as indicated by a dash line. Furthermore, pulse shapes of MPCs in Class-III clusters are less distorted than ones in Class-I and Class-II clusters. Multipath clusters arriving at 182.7 ns is dominated by diffraction from a wooden door with d=4.44 cm., and at 203.7 ns and 223.2 ns are distorted by reflection from a concrete wall (d= 19.45 cm.).

Referring to dielectric constants of furniture materials in propagation paths [9-10], properties of dielectric constants with frequency variation are also taken into account, thus simulation at each subband examines pulse distortions from different dielectric constants. The effects of frequency-dependent dielectric constants of materials for individual UWB propagation paths are characterized with results in Fig. 5. Total energies of all simulated MPCs from all 3x3 arrays are computed and normalized at each frequency subband. It can be obviously seen that, total energy variations of each material fluctuate nearly the same in the overall subband; however, there is dramatic variations of total energies in NLOS Case-D propagation channels. This might be due to various obstructions along the long distance of propagation paths which can distort and attenuate the simulated signal strength.

5. Conclusion

This work proposes a modified UWB simulation method which includes generalization of the UWB pulse shape distortion caused by different mechanisms of single and multiple reflection and diffraction. Furthermore, the spatio-temporal UWB CIR model is also implemented specifically for various clusters, both for LOS and NLOS cases. In order to taken into account frequency-dependent effects on multipath signals, distorted UWB multipath pulses are generalized at each frequency subband regarding to TOAs, AODs, AOAs and dominant obstruction clusters classified for each scenario case. Furthermore, results of frequency-dependent distortions present variations of normalized total energies of all simulated pulse signals. Comparing between all scenario cases, NLOS Case-D presents the worst case of total energy frequency-variation as propagating through the longest distance and scattering from various obstructions.

References

[1] A. Saleh and R. A. Valenzuela, "A statistical model for indoor multipath propagation," *IEEE J. Sel. Areas Commun.*, vol. 5, no. 2, pp. 128–137, Feb. 1987.

[2] C. Chong, Y. Kim, and S. S. Lee, "A modified S-V clustering channel model for the UWB indoor residential environment," in *IEEE Proc. on Vehicular Technology Conference 2005*, Stockholm, Sweden, May 2005, pp 58-62.

[3] Q. H. Spencer, B. D. Jeffs, M. A. Jenson, and A. L. Swindlehurst, "Modeling the statistical time and angle of arrival characteristics of an indoor multipath channel," *IEEE J. Sel. Areas. Commun.*, vol. 18, no.3, pp. 347- 359, Mar. 2000.

[4] Y. Chen and V. K. Dubey, "Dynamic simulation model of indoor wideband directional channels," *IEEE Trans. Veh. Technol.*, vol. 55, no. 2, pp. 417- 430, Mar. 2006.

[5] R. C. Qiu, "A generalized time domain multipath channel and its application in ultra-wideband (UWB) wireless optimal receiver – part III: system performance analysis," *IEEE Trans Wireless Commun.*, vol. 5, no. 10, pp. 2685-2695, Oct. 2006.

[6] R. C. Qiu, "A generalized time domain multipath channel and its application in ultra-wideband (UWB) wireless optimal receiver – part II: physics-based system analysis," *IEEE Trans Wireless Commun.*, vol. 3, no. 6, pp. 2312-2324, Nov. 2004.

[7] K. Haneda, J. Takada, and T. Kobayashi, "Cluster properties investigated from a series of ultrawideband double directional propagation measurements in home environments," *IEEE Trans. Antennas Propag.*, vol. 54, no. 12, pp. 3778- 3788, Dec. 2006.

[8] R. J. M. Cramer, R. A. Scholtz, and M. Z. Win, "Evaluation of an ultra-wide-band propagation channel," *IEEE Antennas Propag.*, vol. 50, no. 5, pp. 561- 570, May. 2002.

[9] A. Safaai-Jazi, S. M. Riad, A. Muqaibel, and A. Bayram, "Ultra-wideband propagation measurements and channel modelling," Time domain and RF measurement Lab., Virginia Polytechnic Institute and State University, VA Rep. 24061-0111, 2002.

[10] A. Muqaibel, A. Safaai-Jazi, A. Bayram, A.M. Attiya, and S. M. Riad, " Ultrawideband through-the-wall propagation," *IEE Proc. Microw. Antennas Propag.*, vol. 52, no. 6, pp. 581- 588, Dec. 2005.